MODELLING AND TESTING OF AN ARCHIMEDES HYDRO TURBINE

ME 407 Mechanical Engineering Group Project 1

Semester 7 : November 2019

By

M.V.R.L.D.B.Ariyarathna (E/14/022)

M.H.Azher (E/14/027)

This report is submitted for the completion of the requirements of the course ME 407 which is offered for the Degree of Bachelor of the Science of Engineering (B.Sc. Eng) of the University of Peradeniya

Department of Mechanical Engineering

Faculty of Engineering

University of Peradeniya

Sri Lanka

MODELLING AND TESTING OF AN ARCHIMEDES HYDRO TURBINE

by

M.V.R.L.D.B.Ariyarathna

M.H.Azher

Supervised by

Dr. S.P.Gunawardana

DECLARATION

We declare that this report does not incorporate, without acknowledgement, any material previously submitted for any other Degree or Diploma to the best of my knowledge and belief, it does not contain any material previously published or written by another person or myself except where due references are made. It has not been accepted for any other course and is not being concurrently submitted to any other person.

Signature of candidate	Signature of candidate
.....	.....
Name of candidate	Name of candidate
.....	.....

Date: ...../...../.....

Countersigned by:

Signature of supervisor Date: ...../...../.....

.....

Name of Supervisor

.....

ACKNOWLEDGEMENT

We wish to express our sincere gratitude to our supervisor, Dr. S.P.Gunawardana for guiding us through difficult steps of our project and helping us to understand the method of conducting a research for solving a problem.

Also, we are forever grateful to Dr. L.N.Wickramarathna, coordinator of the course for planning and executing the course and guiding us through necessary procedures.

ABSTRACT

The scope of this project explores the numerical modelling and tasting of a Archimedes hydro turbine. The project focuses on investigating on various techniques of modelling the device using the software ‘Star CCM+’ and selecting the best configurations for this level of simulation. Initially the turbine was tested under completely submerged fluid flow, to check the effectiveness of the overset mesh. Afterwards different geometric models of the turbine were modeled under Eularian multi-phase flow. Since convergence was not achieved during the initial trials, turbulence models were changed. To increase the accuracy of results, number of cells in the mesh were increased. Finally, the performance of all three geometric models were compared.

TABLE OF CONTENTS

DECLARATION i
ACKNOWLEDGEMENT ii
ABSTRACT ivii
LIST OF FIGURES v
ABBREVIATIONS ivi

Chapter 1 INTRODUCTION 1
Chapter 2 LITERATURE SURVEY 3
Chapter 3 METHODOLOGY 4
Chapter 4 MESHING 5
4.1 Overset mesh 5
4.2 Dynamic Fluid Body Interactions (DFBI) 9
4.3 Dynamic Overset Behavior 9
Chapter 5 Turbulence Models 10
5.1 Reynolds-averaged Navier-Stokes equations and classical turbulence models 10
5.1.1 k-Epsilon Model 11
5.1.2 k-Omega Model 13
5.1.3 Turbulence Suppression 14
Chapter 6 Initial and Boundary Conditions 15
6.1 Initial Conditions 15
6.2 Boundary Conditions 16
Chapter 7 Results 19
7.1 3 Start, 45 degree pitch angle turbine 19
7.1.1 Angular velocity 20
7.1.2 Body moment 20
7.2 6 Start, 75 degree pitch angle turbine 21
7.2.1 Angular velocity 22
7.2.2 Body moment 22
7.3 Variable pitch angle, 3 start turbine 23
7.2.1 Angular velocity 23
7.2.2 Body moment 24
Chapter 8 DISCUSSION 25
Chapter 9 CONCLUSION 27
Chapter 10 FUTURE WORK 28
Chapter 11 REFERENCE 29

LIST OF FIGURES

Figure 1:Components of the Archimedes screw turbine power generation 1
Figure 2:Overset Region 6
Figure 3:Overset Region-Turbine Wall 6
Figure 4:Overset Mesh 7
Figure 5:Types of cells in the overset mesh 8
Figure 6:Fluid Domain Inlet 17
Figure 7:Fluid Domain Outlet 17
Figure 8:Fluid Domain Wall 18
Figure 9:3 Start, 45 degree pitch angle turbine under fluid flow 19
Figure 10:Variation of angular velocity 3 start turbine with time 20
Figure 11: Variation of body moment 3 start turbine with time 20
Figure 12:6 Start, 75 degree pitch angle turbine under fluid flow 21
Figure 13:Variation of angular velocity of 6 start turbine with time 22
Figure 14:Variation of body moment of 6b start turbine with time 22
Figure 15:Operation of variable pitch angle turbine under fluid flow 23
Figure 16:Variation of Angular Velocity of Variable Pitch Turbine with time 23
Figure 17:Variation of Body Moment of Variable Pitch Turbine with time 24
Figure 18:Comparision of angular velocity 25
Figure 19:Comparison of body moment 26

ABBREVIATIONS

DFBI	Dynamic Fluid Body Interactions
VOF	Volume of Fluid
CFD	Computational Fluid Dynamics
k	Turbulent Kinetic Energy
ε	Turbulent Dissipation Rate
ϑ	Turbulent Velocity scale
ℓ	Turbulent Length scale
ρ	Fluid Density
ω	Turbulence Frequency
μ_t	Eddy Viscosity
U_{ref}	Reference Velocity
T_i	Turbulence Intensity

1 INTRODUCTION

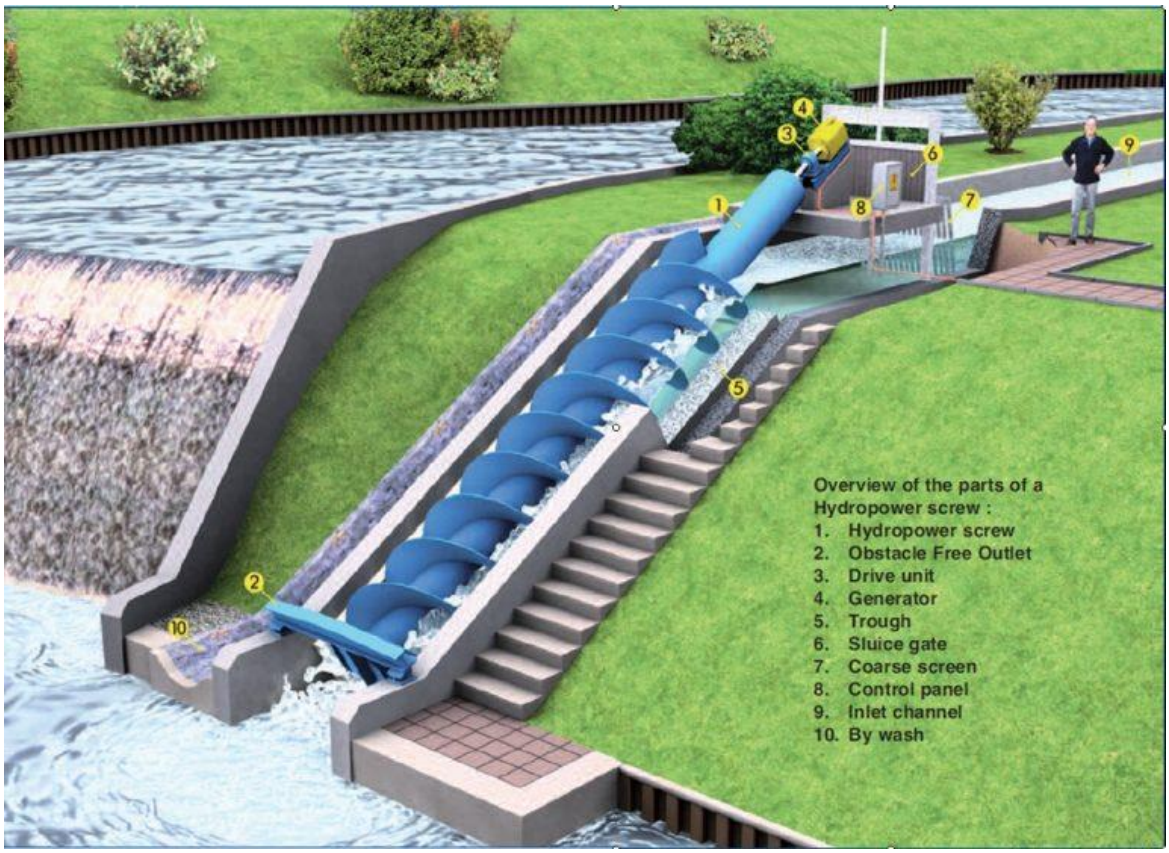

Figure 1:Components of the Archimedes screw turbine power generation

The Archimedes screw pump was invented by Archimedes as a means of elevating water for low to medium heights (approximately 1 meter). Later it was mechanically driven to pump water. Initially pumps were powered manually, either by human or animal labor, in some cases wind power had also been used. Later this concept was reversed to obtain power from a flowing water source with low head.

Archimedes hydro turbine specialize in maximizing efficiency in low head s and high flow rates. A single Archimedes turbine can generate power between 10 kW to 15kW. Usually hydro power plants have multiple sets of turbines coupled to generate power between 100 kW to 350 kW.

At an era where limited fossil fuel reserves and climate change are pressing issues, renewable energy has become the most viable solution. And amongst those solutions

the Archimedes turbine has taken prominence due to its minimal effects on the environment, since it is ‘Fish friendly’ and due to the minimal infrastructure requirements.

The software primarily used to model the turbine geometrically and numerically were ‘SOLIDWORKS’ and ‘Star CCM+’ respectively. Star CCM+ is an industrially used software to solve continuum mechanics problems such as computational fluid dynamics.

2 LITERATURE SURVEY

A review of ‘Simplified theory of Archimedean screws’ by Gerald Muller compares Archimedes turbines to the hydrostatic pressure machine. The mathematical model derived through the comparison shows that the performance of the turbine solely depends on its geometry. Due to this important discovery prominence of the project was given to testing different geometries of the turbine at the same condition. Thus, the following geometries were selected.

Pitch angle 45˚, 3 start turbine, is the most commonly used geometry in commercial applications. Although it has a favorable efficiency due to its high attack angle the turbine is prone to vibrations. To reduce the high attack angle a pitch angle 75˚model was considered. Since the power extraction reduces due to low attack angle the number of starts were increased in the considered model. Due to the complexity of the model manufacturing cost is high, thus to compromise on all the above mentioned shortcomings a variable pitch model was also selected for testing.

The numerical model approach towards tackling this problem was learnt through ‘Introduction to computational fluid dynamics by H.K. Verteeg and W.Malalasekara’. It was understood that the overset mesh is the best meshing technique to solve the numerical model. The necessary initial conditions and turbulence models to be applied on the numerical model were gathered. The best turbulence model for turbo machinery is k-Omega model but has the risk of delivering divergent results.

3 METHODOLOGY

As this project was aimed to develop a numerical model and testing of Archimedes turbine it was decided to use ‘Star CCM+’ software which is commercially used CFD toolbox. Since it is user friendly and order of setting up the simulation does not interfere with the final result, ‘Star CCM+’ was selected. For 3D modeling ‘Solidworks’ was used as it is also user friendly and a highly verified software.

First, the function of the overset mesh was validated using fully submerged fluid flow. Once the meshing technique was verified it was then applied to Eularian multi-phase volume of fluid flow which consists of both air and water.

As the results were not converged the turbulence model was changed from k-Omega to k-Epsilon model and turbulence suppression was applied to suppress turbulence in the near wall areas. The plots of the physical quantities angular velocity, angular acceleration, body moment and body rotational energy were obtained for all three geometries. Finally the results of the three geometries were compared.

4 MESHING

4.1 Overset mesh

STAR-CCM+ includes geometry tools, preprocessing, solvers, post-processing and optimization delivered from a single integrated user interface. The individual grids are prepared using the standard meshing process in STARCCM+, and you can implement the overset mesh between grids in a few simple and automated steps:

1. Two or more individual regions are created: a region with the background geometry (background region) and separate regions surrounding the bodies of interest (Overset regions)

2. The regions are meshed separately. There will be a zone where computational cells overlap between regions

3. The outer boundary of the overset body is set to overset mesh boundary condition; the regions are selected together and an overset interface is created between them

4. As the overset body moves within the background region, the overlapping zone will change

5. Information is exchanged between the regions through the overlapping cells

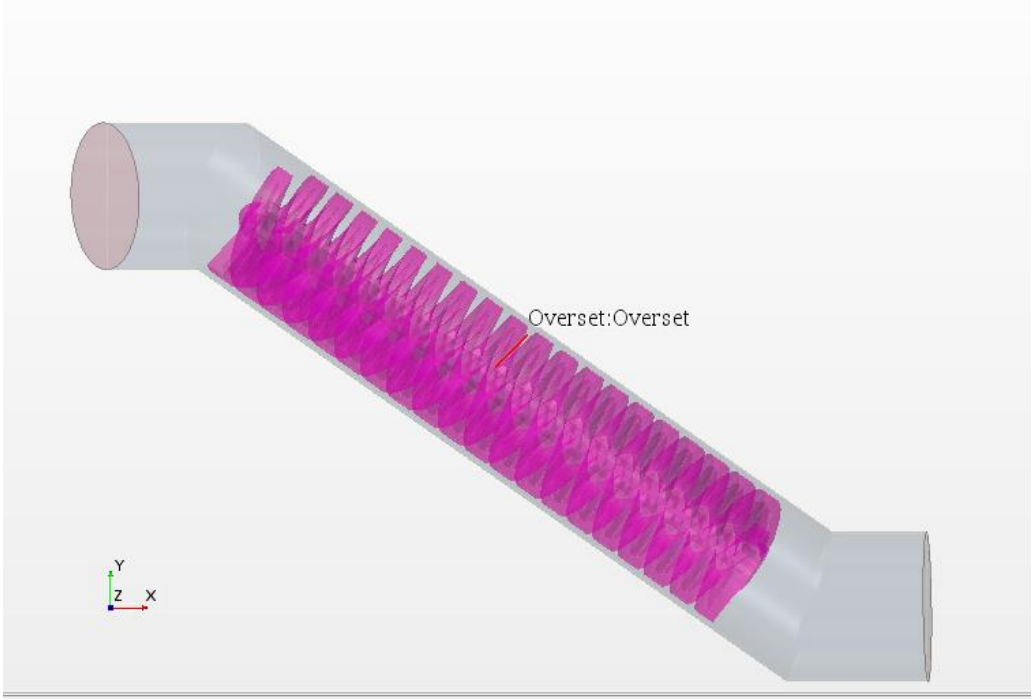

Figure 2:Overset Region

The overset region is created as a shell around the turbine.

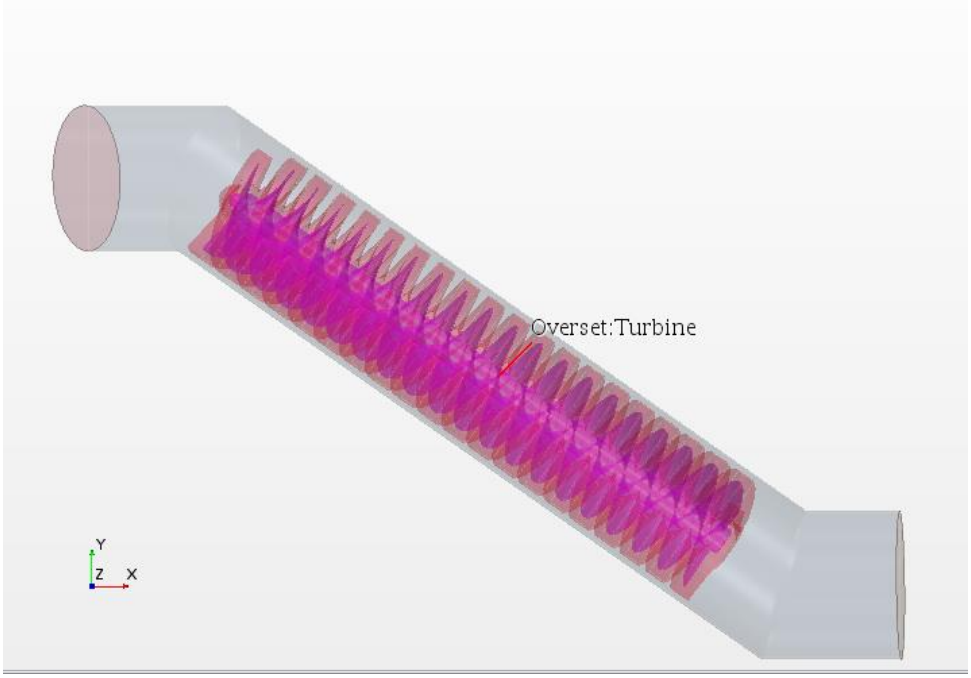

Figure 3:Overset Region-Turbine Wall

Once the overset mesh is created, the hole-cutting process in STAR-CCM+ automatically couples the overset region with the background region through the overset interface. A successful coupling results in a hole being cut out in the background mesh where the overset mesh resides. Cells are marked as active and passive in the coupled simulation. The hole-cutting process follows one of the two approaches:

- Layered approach: A layer of cells along the overset boundary is identified as the donor layer. The immediate cells next to the donors in the background region become acceptors. The cells in the background that are completely covered by the cells in the overset region become inactive

- Global approach: For each cell in the background region, the algorithm verifies whether the cell centroid is inside or outside the overset region. If it is inside the overset region, the cell becomes inactive.

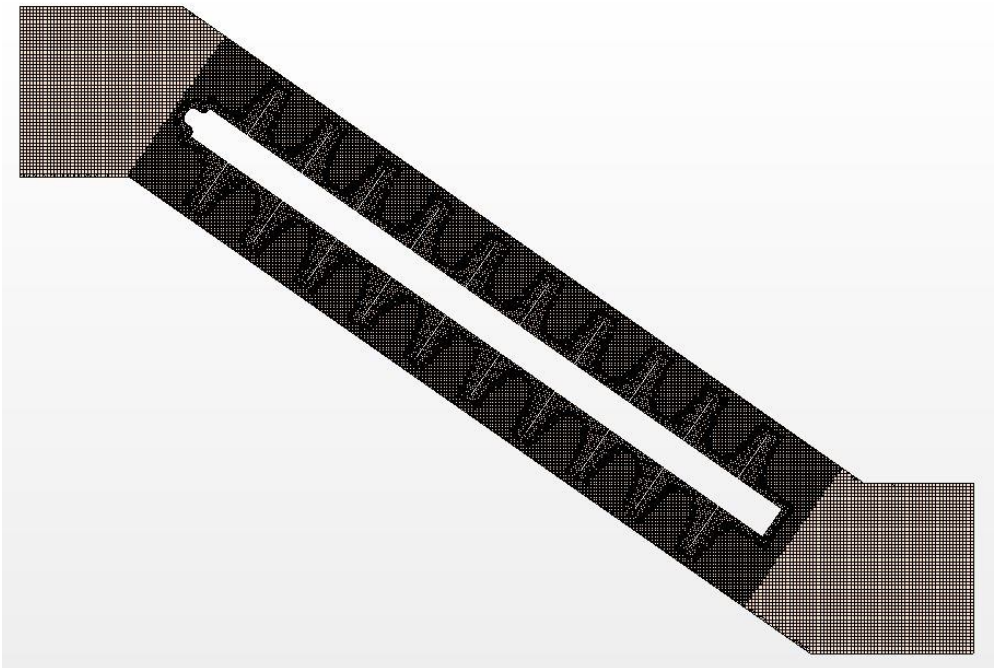

Figure 4:Overset Mesh

Based on the hole-cutting process, four types of cells are identified as shown in Figure3.

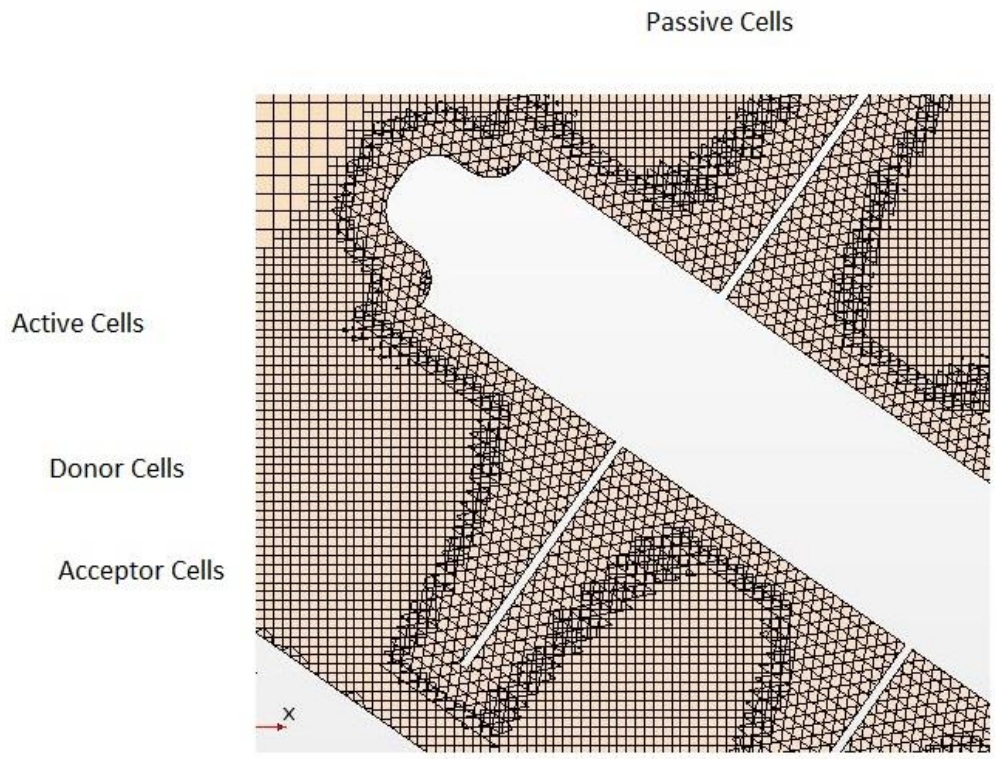

Figure 5:Types of cells in the overset mesh

- Active cells (cyan and yellow): Discretizing governing equations are solved here.
- Passive cells (dark blue): No equations are solved here.
- Donor cells (green): These provide interpolation information to the mesh acceptor cells.
- Acceptor cells (red): The boundary cells that receive information from the donor cells.

The data transfer between the meshes is implicitly coupled, with a solution being computed on all grids simultaneously, leading to improved robustness and convergence. The linear model of data transfer was selected for the numerical model.

4.2 Dynamic Fluid Body Interactions (DFBI)

Dynamic fluid body interaction (DFBI): The DFBI model enables the analysis of objects when their motion is not known a-priori. The motion of the object, which is due to the action of fluids and other forces, is imparted through the overset mesh. The major advantage of this feature in the design process is that it allows you to determine the motion of the objects using simulation, rather than expensive physical testing. The DFBI contact coupling model allows bodies to collide and rebound from contact, which is modeled as a repulsive force.

4.3 Dynamic Overset Behavior

In some applications, the boundary of the overset body can switch between a wall boundary type to an overset boundary type and vice versa depending on the motion. In addition, a background mesh may or may not be necessary depending on the motion. There are also applications in which a background mesh is needed only for a certain part of the motion. Such dynamic overset behavior can be modeled with or without the background mesh. The boundary type is set to wall when the dynamic overset behavior option is activated. This eliminates the need for background regions when they are not necessary, reducing the cell count and the time required for interpolation. The boundary remains as a wall type until it comes in contact with the other region, switching to an overset boundary type when this happens.

5 Turbulence Models

All flows encountered in engineering practice, simple ones, such as two dimensional jets, wakes, pipe flows and flat plate boundary layers, and more complicated three-dimensional ones, become unstable above a certain Reynolds number (UL/v where U and L are characteristic velocity and length scales of the mean flow and v is the kinematic viscosity). At low Reynolds numbers flows are laminar. At higher Reynolds numbers flows are observed to become turbulent. A chaotic and random state of motion develops in which the velocity and pressure change continuously with time within substantial regions of flow.

5.1 Reynolds-averaged Navier-Stokes equations and classical turbulence models

Turbulence models for Reynolds-averaged Navier–Stokes (RANS) equations: attention is focused on the mean flow and the effects of turbulence on mean flow properties. Prior to the application of numerical methods the Navier–Stokes equations are time averaged (or ensemble averaged in flows with time-dependent boundary conditions). Extra terms appear in the time-averaged (or Reynolds averaged) flow equations due to the interactions between various turbulent fluctuations. These extra terms are modelled with classical turbulence models: among the best known ones are the k–ε model and 3.6 the Reynolds stress model. The computing resources required for reasonably accurate flow computations are modest, so this approach has been the mainstay of engineering flow calculations over the last three decades. The main two types of turbulence models used for this project were k-Epsilon model and k-Omega model.

5.1.1 k-Epsilon Model

In flows where convection and diffusion cause significant differences between production and destruction of turbulence, e.g. in recirculating flows, a compact algebraic prescription for the mixing length is no longer feasible. The way forward is to consider statements regarding the dynamics of turbulence. The k–ε model focuses on the mechanisms that affect the turbulent kinetic energy.

It is possible to develop similar transport equations for all other turbulence quantities including the rate of viscous dissipation ε (see Bradshaw et al., 1981). The exact ε-equation, however, contains many unknown and unmeasurable terms. The standard k–ε model (Launder and Spalding, 1974) has two model equations, one for k and one for ε, based on our best understanding of the relevant processes causing changes to these variables. We use k and ε to define velocity scale ϑ and length scale ℓ representative of the large-scale turbulence as follows:

$$\vartheta = k^{1/2} \quad \ell = \frac{k^{3/2}}{\varepsilon}$$

One might question the validity of using the 'small eddy' variable ε to define the 'large eddy' scale ℓ. We are permitted to do this because at high Reynolds numbers the rate at which large eddies extract energy from the mean flow is broadly matched to the rate of transfer of energy across the energy spectrum to small, dissipating, eddies if the flow does not change too rapidly. If this was not the case the energy at some scales of turbulence could grow or diminish without limit. This does not occur in practice and justifies the use of ε in the definition of ℓ. Applying dimensional analysis we can specify the eddy viscosity as follows:

$$\mu_t = C\rho\vartheta\ell = \rho C_\mu \frac{k^2}{\varepsilon}$$

Where, Cμ is a dimensionless constant. The standard k–ε model uses the following transport equations for k and ε:

$$\frac{\partial(\rho k)}{\partial t} + \mathrm{div}(\rho k \mathbf{U}) = \mathrm{div}\left[\frac{\mu_t}{\sigma_k}\,\mathrm{grad}\ k\right] + 2\mu_t S_{ij} \,.\, S_{ij} - \rho\varepsilon$$

$$\frac{\partial(\rho\varepsilon)}{\partial t} + \text{div}(\rho\varepsilon\mathbf{U}) = \text{div}\left[\frac{\mu_t}{\sigma_\varepsilon}\,\text{grad}\,\varepsilon\right] + C_{1\varepsilon}\frac{\varepsilon}{k}2\mu_t S_{ij}\,.\,S_{ij} - C_{2\varepsilon}\rho\frac{\varepsilon^2}{k}$$

In words the equations are,

Rate of change of k or ε	+	Transport of k or ε by convection	=	Transport of k or ε by diffusion	+	Rate of production of k or ε	−	Rate of destruction of k or ε

The equations contain five adjustable constants: Cμ , σk , σε , C1ε and C2ε . The standard k–ε model employs values for the constants that are arrived at by comprehensive data fitting for a wide range of turbulent flows:

$$C_\mu = 0.09 \quad \sigma_k = 1.00 \quad \sigma_\varepsilon = 1.30 \quad C_{1\varepsilon} = 1.44 \quad C_{2\varepsilon} = 1.92$$

Advantages:

- Simplest turbulence model for which only initial and/or boundary conditions need to be supplied
- Excellent performance for many industrially relevant flows
- Well established, the most widely validated turbulence model

Disadvantages:

- More expensive to implement than mixing length model (two extra PDEs)
- Poor performance in a variety of important cases such as:
  - (i) some unconfined flows
  - (ii) flows with large extra strains (e.g. curved boundary layers, swirling flows)
  - (iii) rotating flows
  - (iv) flows driven by anisotropy of normal Reynolds stresses (e.g. fully developed flows in non-circular ducts)

5.1.2 k-Omega Model

In the k–ε model the kinematic eddy viscosity v_t is expressed as the product of a velocity scale ϑ = k and a length scale ℓ = k 3/2/ε. The rate of dissipation of turbulence kinetic energy ε is not the only possible length scale determining variable. In fact, many other two-equation models have been postulated. The most prominent alternative is the k–ω model proposed by Wilcox (1988, 1993a,b, 1994), which uses the turbulence frequency ω = ε/k (dimensions s−1) as the second variable. If we use this variable the length scale is $\ell = k^{0.5}/\omega$. The eddy viscosity is given by.

$$\mu_t = \rho k / \omega$$

The Reynolds stresses are computed as usual in two-equation models with the Boussinesq expression:

$$\tau_{ij} = -\rho \overline{u_i' u_j'} = 2\mu_t S_{ij} - \frac{2}{3}\rho k \delta_{ij} = \mu_t \left(\frac{\partial U_i}{\partial x_j} + \frac{\partial U_j}{\partial x_i} \right) - \frac{2}{3}\rho k \delta_{ij}$$

The transport equation for k and ω for turbulent flows at high Reynolds is as follows:

$$\underbrace{\frac{\partial(\rho k)}{\partial t}}_{\text{(I)}} + \underbrace{\operatorname{div}(\rho k \mathbf{U})}_{\text{(II)}} = \underbrace{\operatorname{div}\left[\left(\mu + \frac{\mu_t}{\sigma_k} \right) \operatorname{grad}(k) \right]}_{\text{(III)}} + \underbrace{P_k}_{\text{(IV)}} - \underbrace{\beta^* \rho k \omega}_{\text{(V)}}$$

Where,

$$P_k = \left(2\mu_t S_{ij} \,.\, S_{ij} - \frac{2}{3}\rho k \frac{\partial U_i}{\partial x_j} \delta_{ij} \right)$$

is the rate of production of turbulent kinetic energy and

$$\frac{\partial(\rho\omega)}{\partial t} + \operatorname{div}(\rho\omega\mathbf{U}) = \operatorname{div}\left[\left(\mu + \frac{\mu_t}{\sigma_\omega} \right) \operatorname{grad}(\omega) \right]$$

$$+ \gamma_1 \left(2\rho S_{ij} \,.\, S_{ij} - \frac{2}{3}\rho\omega \frac{\partial U_i}{\partial x_j} \delta_{ij} \right) - \beta_1 \rho \omega^2$$

Or in words

Rate of change of k or ω	+	Transport of k or ω by convection	=	Transport of k or ω by turbulent diffusion	+	Rate of production of k or ω	−	Rate of dissipation of k or ω

The model constants are as follows:

$$\sigma_k = 2.0 \quad \sigma_\omega = 2.0 \quad \gamma_1 = 0.553 \quad \beta_1 = 0.075 \quad \beta^* = 0.09$$

5.1.3 Turbulence Suppression

In the turbulence suppression model turbulence at the near wall regions are suppressed by reducing the value of above constants in the k-Epsilon and k-Omega turbulence models.

Turbulence suppression is achieved in a region as follows:

1. Setting the turbulent eddy viscosity and/or the Reynolds stresses to zero
2. Setting the production terms in the turbulence transport equations to zero
3. Not using wall functions to compute wall shear stress or heat flux, but using the laminar flow transport equations instead

6 Initial and Boundary Conditions

6.1 Initial Conditions

Initial conditions in a physics continuum specify the initial field data for the simulation. For steady-state simulations, the converged solution should be independent of the initial field. However, the path to convergence, and hence the computational effort that is required to reach convergence, is affected. Therefore, choose the initial conditions and values judiciously, particularly when the physics is complex. Each model requires sufficient information for the primary solution data for the primary variables that are associated with the model to be set. In most cases, the initial conditions are set up directly. For some models, such as turbulence, there is the option of specifying the information in a more convenient form (turbulence intensity and turbulent viscosity ratio instead of turbulent kinetic energy and turbulent dissipation rate).

Examples of initial conditions are:

- Pressure
- Temperature
- Velocity components
- Turbulence quantities

Pressure –

The pressure is usually the gauge pressure since this an open flow gauge pressure is zero. But to avoid floating point errors 8 Pa was used.

Temperature –

Temperature of 25 Celsius was used.

Velocity Components –

To avoid back flows of the simulation a reasonable value 0.8 m/s was used.

Turbulence Quantities –

Initially the method of turbulence specification is selected. For the purpose of modeling K + Epsilon specification method was selected. Although the exact value for these quantities cannot be determined easily, a rough estimation was

done. K being turbulent kinetic energy nd Epsilon being Turbulence dissipation rte.

$$k = \frac{2}{3}(U_{ref}T_i)^2$$

In the above equation U_{ref} is the reference velocity and T_i is the turbulence Intensity. U_{ref} value of 0.8 m/s was used(s mentioned above) and T_i value of 0.05 ws used (an ideal value used for turbo machinery in CFD). Solving the equation gave the k value of 0.001.

$$\varepsilon = C_\mu^{3/4}\frac{k^{3/2}}{l}$$

In the above equation ℓ is the turbulence length scale and is calculated s ℓ = 0.07 ℓ and C_μ is constant of the value 0.09. Solving the equation gives us the epsilon value of 0.004.

6.2 Boundary Conditions

STAR-CCM+ provides a wide range of conditions with which you can describe how flow behaves as it meets or passes through the boundaries of the solution domain. Setting these conditions correctly is a vital step in achieving a successful flow solution. For flow simulations, STAR-CCM+ requires that you set quantities and choices on the following boundary types:

- Velocity Inlet
- Mass Flow Inlet
- Stagnation Inlet
- Free Stream
- Wall
- Pressure Outlet
- Outlet

Velocity Inlet –

The face that the fluid enters the system

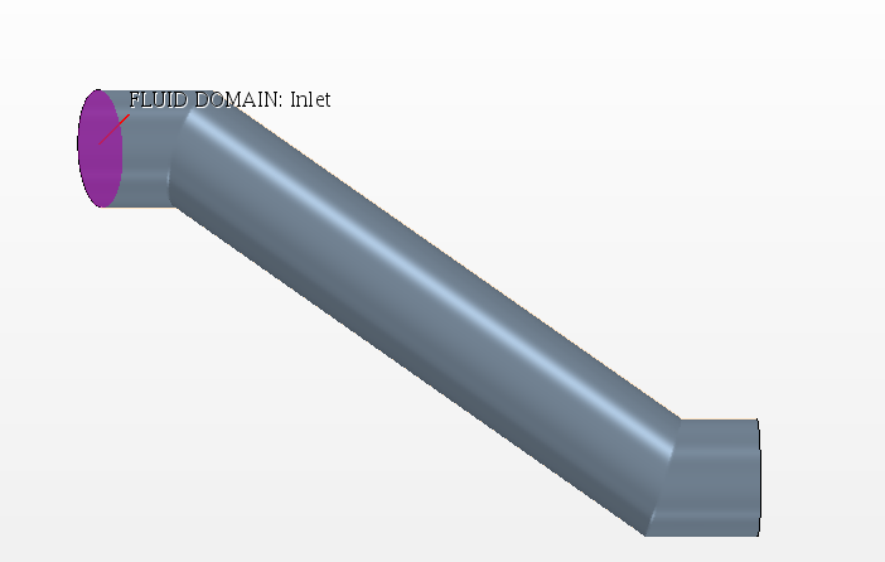

Figure 6:Fluid Domain Inlet

Pressure outlet –

The face that the fluid exits the system

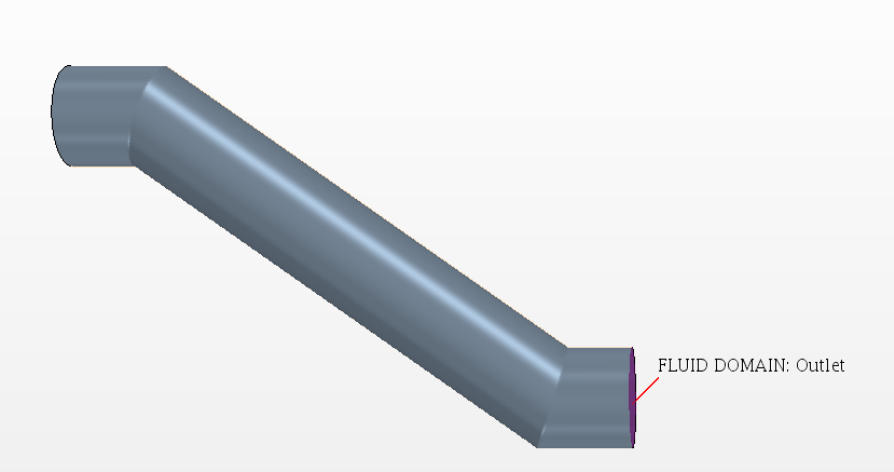

Figure 7:Fluid Domain Outlet

Wall –

Defines how a wall surface acts on a fluid passing across it.

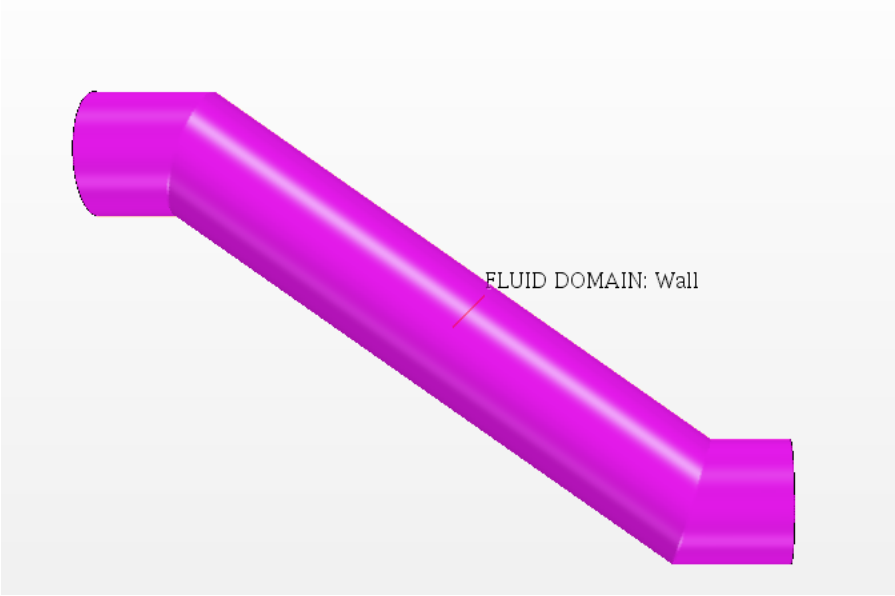

Figure 8:Fluid Domain Wall

7 Results

First, all three models were tested at no load conditions to observe the behavior of turbines at steady state conditions.

7.1 3 Start, 45 degree pitch angle turbine

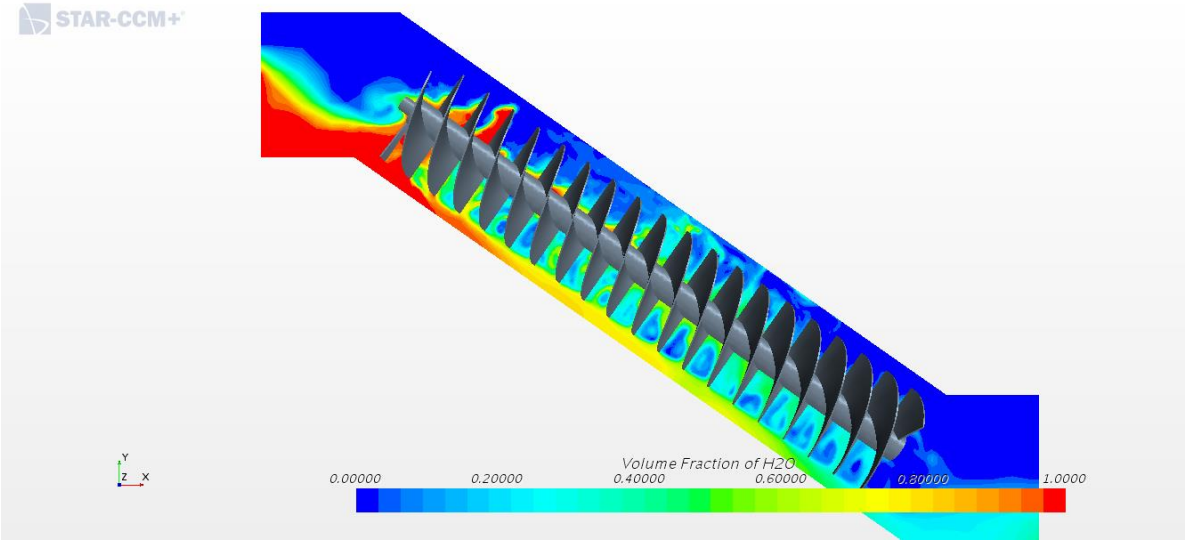

Figure 9:3 Start, 45 degree pitch angle turbine under fluid flow

As it was the first model to be tested the simulation time was set to be 8 seconds. The initial conditions was set as above and the following results were obtained.

7.1.1 Angular velocity

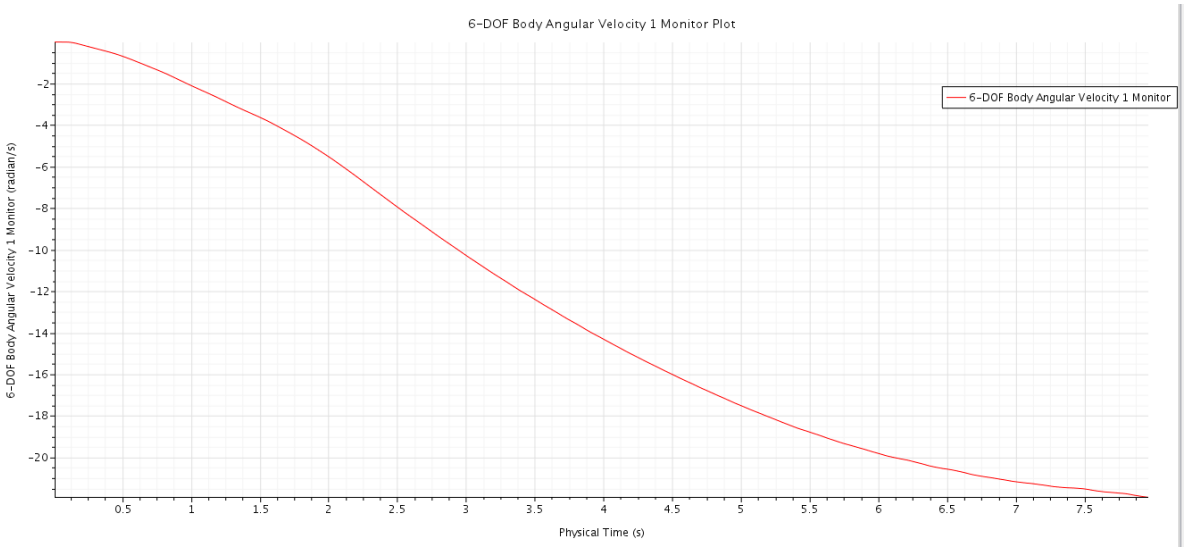

Figure 10:Variation of angular velocity 3 start turbine with time

As per the results obtained the angular velocity looks to converge just above 20 rad/s and the convergence begins approximately at 7.5s.

7.1.2 Body moment

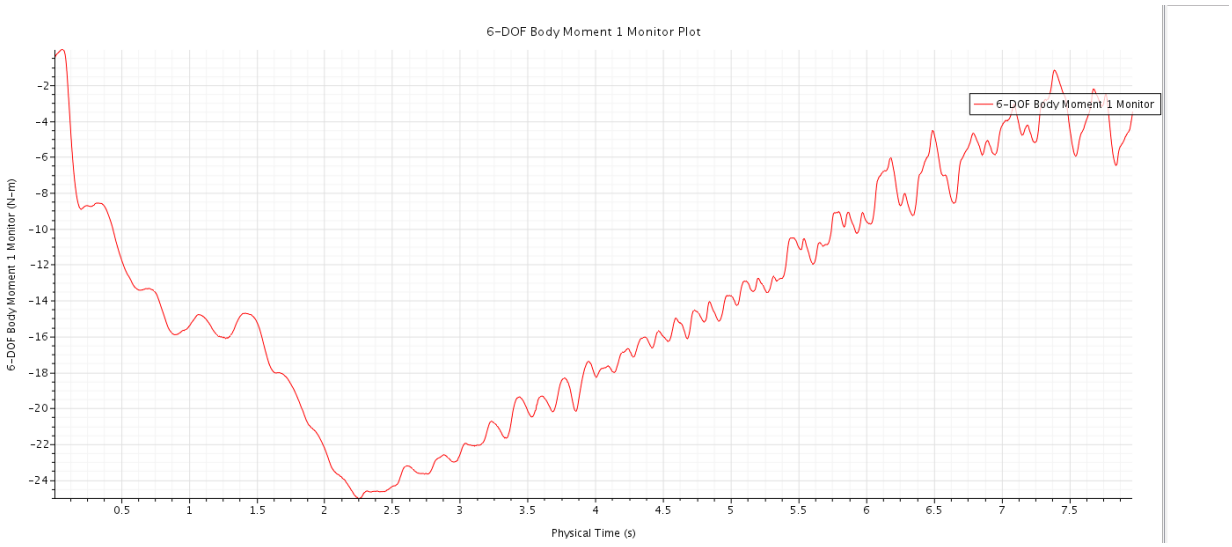

Figure 11: Variation of body moment 3 start turbine with time

As per figure 6, the body moment approaches magnitude zero at steady state but still show subtle variances above and below the zero moment line. It could be predicted that this variances would continue. A vague understanding of the turbine's vibrations could be obtained from the body moment curve

7.2 6 Start, 75 degree pitch angle turbine

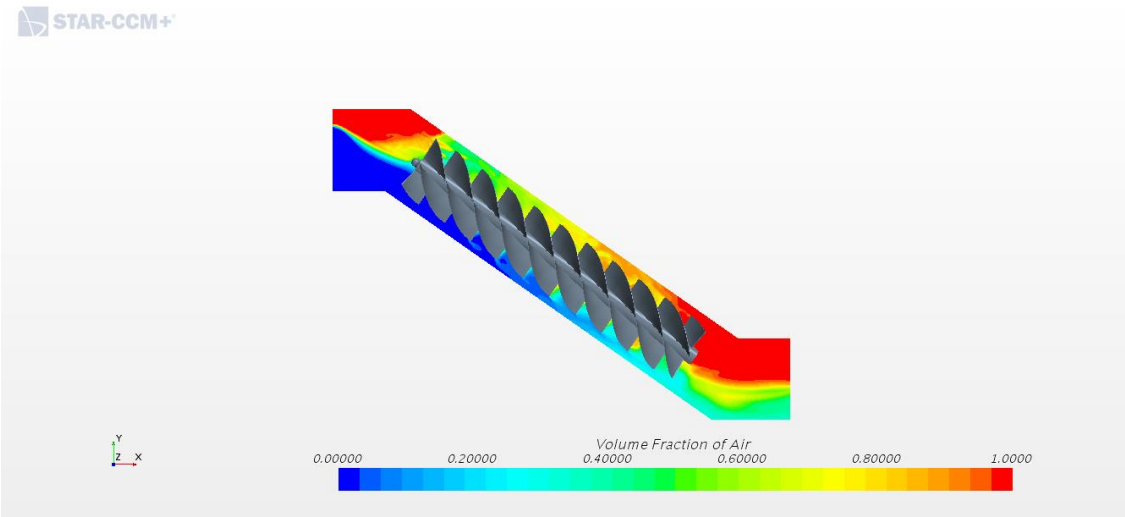

Figure 12:6 Start, 75 degree pitch angle turbine under fluid flow

As this geometry has a low attack angle and higher number of starts, a higher margin of time was added to the simulation so that the steady state could be studied.

7.2.1 Angular velocity

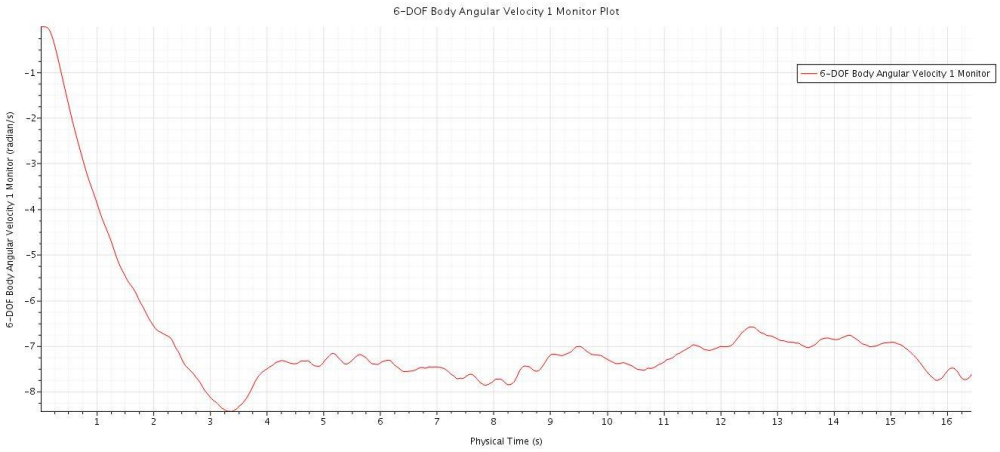

Figure 13:Variation of angular velocity of 6 start turbine with time

According to the plot angular velocity reaches a maximum of 8.5 rad/s and experiences a slight drop, where the angular velocity is maintained around 7.5 rad/s after 3.5 s.

7.2.2 Body moment

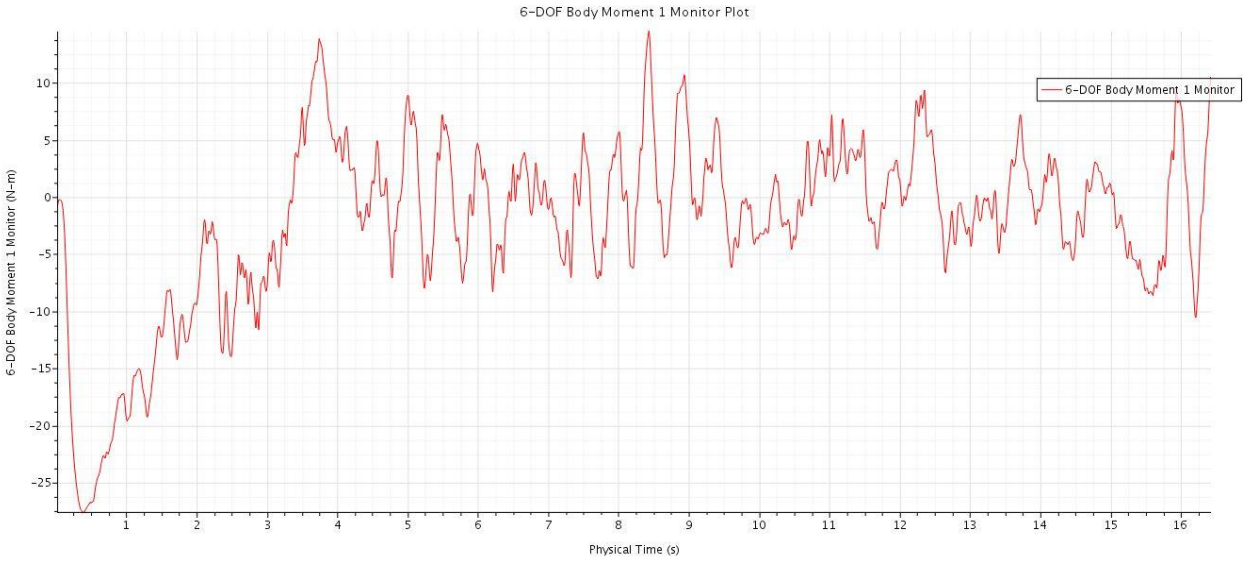

Figure 14:Variation of body moment of 6b start turbine with time

The variation of body moment about the zero level is significant as depicted in the plot. Therefore, the smooth operation of the turbine is questionable.

7.3 Variable pitch angle, 3 start turbine

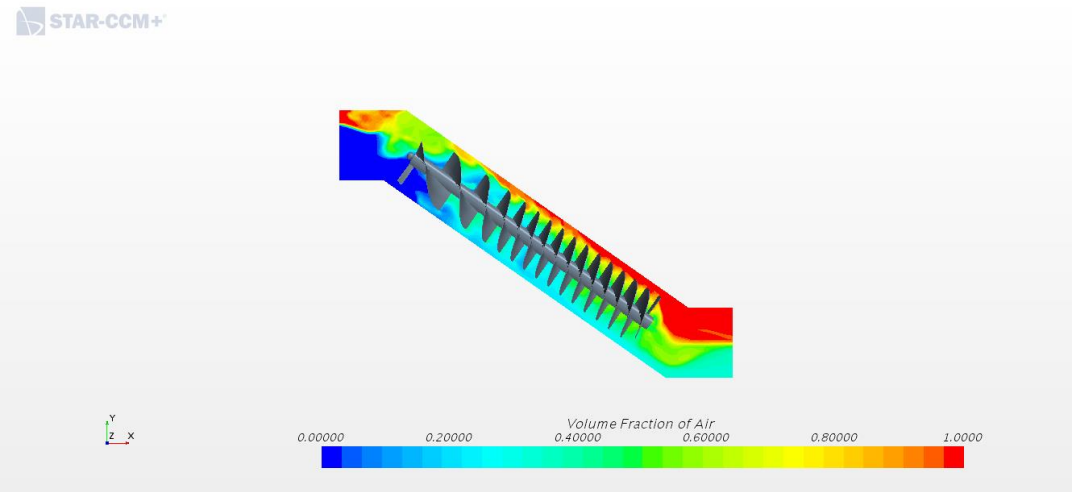

Figure 15:Operation of variable pitch angle turbine under fluid flow

Since, the performance of the turbine changes with the velocity of fluid flow the variable pitch turbine was designed to obtain maximum efficiency over a wider range of velocities.

7.2.1 Angular velocity

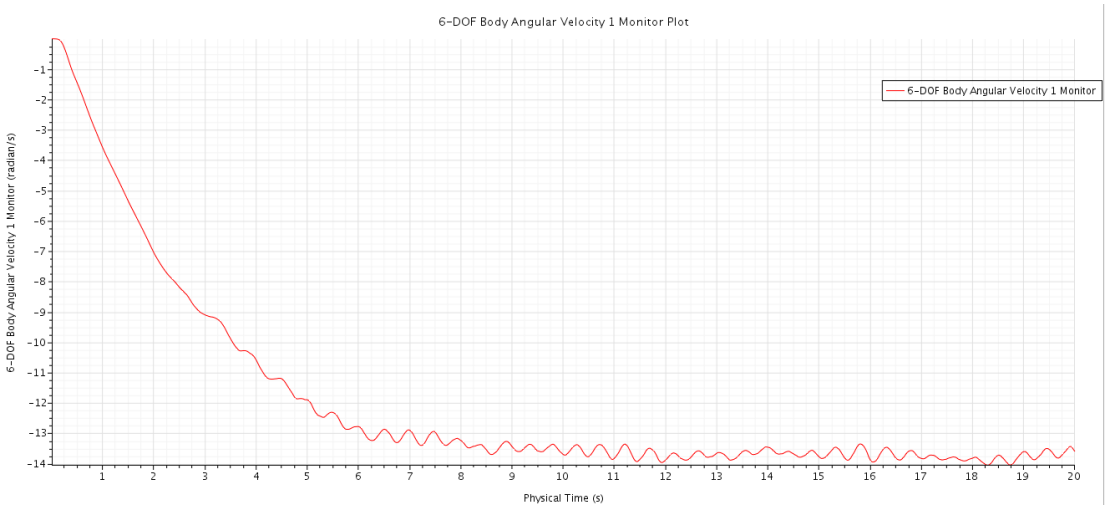

Figure 16:Variation of Angular Velocity of Variable Pitch Turbine with time

As per the plot angular velocity reaches a maximum magnitude of 14 rad/s and maintains that level. Although slight fluctuations could be seen the angular velocity plot is relatively smooth.

7.2.2 Body moment

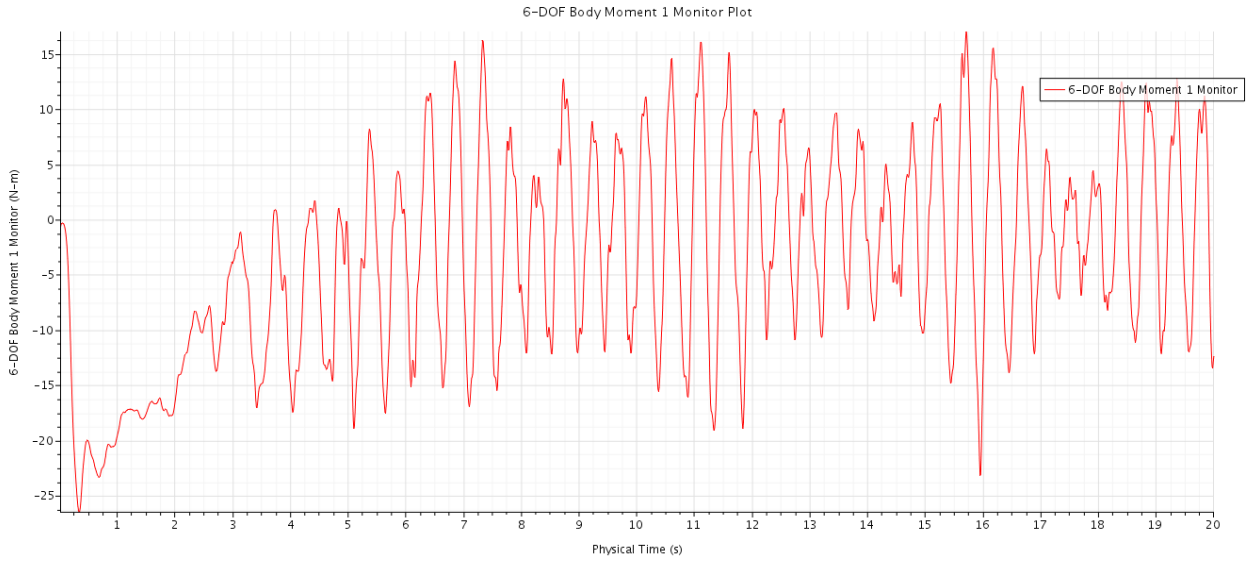

Figure 17:Variation of Body Moment of Variable Pitch Turbine with time

As expected in the variable pitch model, due to the disturbances caused the model exhibits high fluctuations about the zero level**.**

8 DISCUSSION

Since the exact power performance cannot be determined at no load conditions, comparison of the angular velocity plots gives us a rough understanding of the turbine performance.

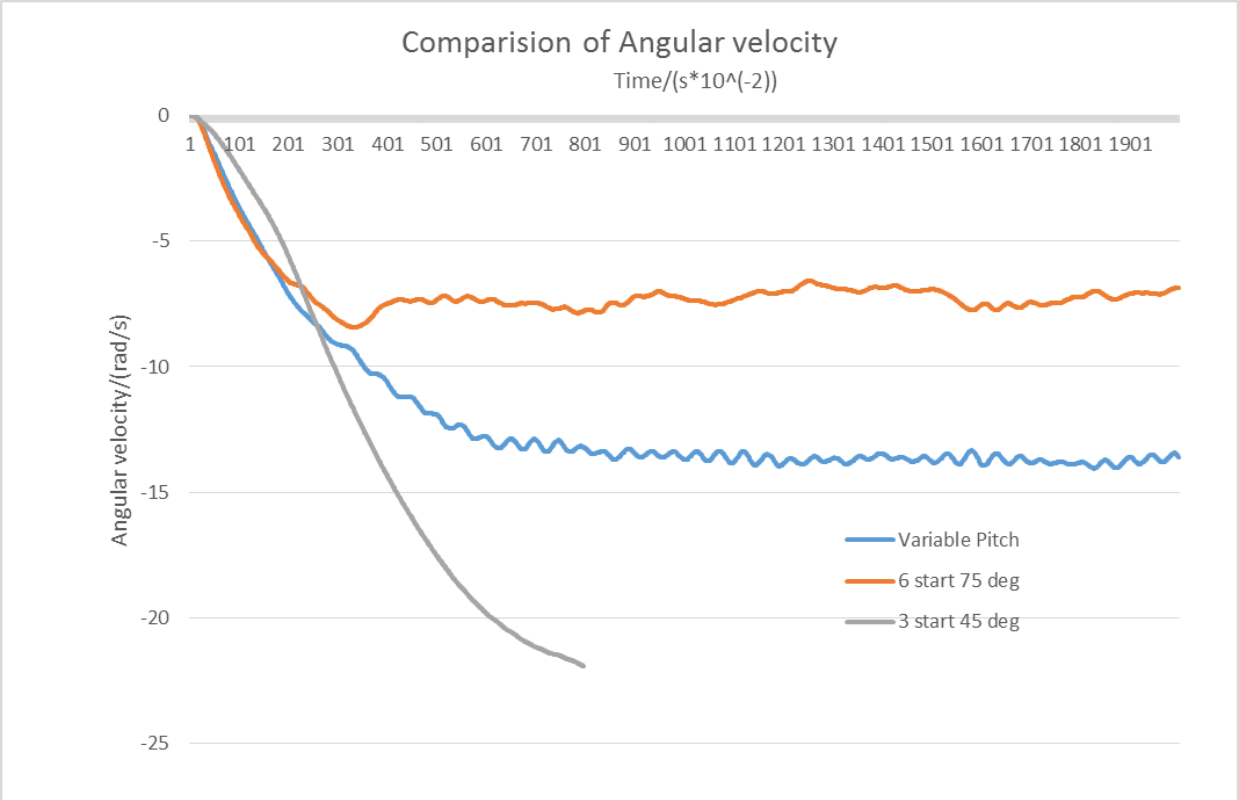

Figure 18:Comparision of angular velocity

At the first glance it could be seen that the 6 start turbine approaches steady state before the other two. In relation to fluctuations of angular velocity the variable pitch turbine exhibits slight fluctuations of greater frequency in comparison to the other turbines. As per the current observations 3 start turbine has the smoothest operation. The 3 start turbine has the highest angular velocity at steady state at no load conditions. This could suggest that the 3 start 45 degree turbine has the best performance but it could not be verified without experimental data at loaded conditions.

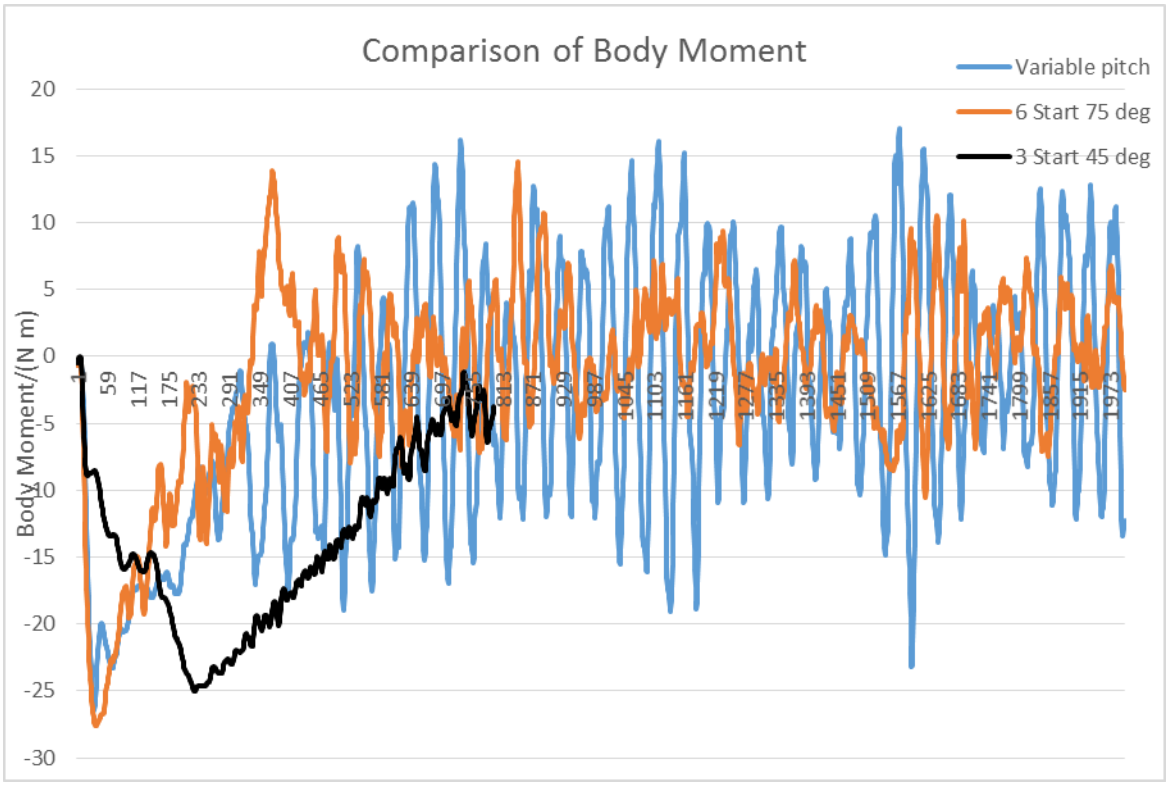

Figure 19:Comparison of body moment

All rotating devices produce vibrations and that is an important aspect when it comes to selecting a good turbine. By studying body moment plots the tendency towards vibrations could be predicted. To reflect the results obtained by the angular velocity plots, the body moment plots also show that the 6 start turbine reaches the steady state before the other two. By comparing body moment fluctuations of the turbines it could be verified that the variable pitch turbine is most prone to vibrations while 45 degree 3 start turbine is the least prone to vibrations.

9 CONCLUSION

By comparing the results obtained at no load conditions the, 45 degree 3 start turbine seems to be the most viable option. Although it reaches steady state after the other turbines the angular velocity and body moment performances are promising. Which is to say that the power extraction of the turbine is at a significant level while the vibrations are negligible. It should be noted that these results were obtained at no load conditions and it might change at loaded conditions.

10 FUTURE WORK

After obtaining results at no load conditions, next step of the project is to obtain results at loaded condition. Afterwards, the turbines will be tested with a range of fluid flow rates. Then, by obtaining this set of data the turbine which provides the maximum efficiency will be chosen. Since one turbine cannot perform at maximum efficiency at all conditions, the most viable turbine at the given condition will be chosen.

11 REFERENCE

1) Verteeg, H.K., and Malalasekara, W. (1995) : *Introduction to Computational Fluid Dynamics*, Second Edition, Chapter 3: Turbulence and its modeling; pg 40-115.

2) Rohmer J., Knittel D., Sturtzer G., Flieller D., Renaud J. (2016) : *Modeling and experimental results of an Archimedes Screw Turbine*, Renewable Energy: Volume 94, Pages 136-146.

3) Müller G., and Senior J. (2009): *Simplified Theory of Archimedean Screws*, journal of Hydraulic Research Vol. 47, No.5, pp 666-669 DOI:10.3826/jhr.2009.3475.

4) Lisicki M., Lubitz W., and Taylor G.W. (2016): *Optimal design and operation of Archimedes Screw Turbines Using Bayesian Optimization*, Applied Energy, Vol. 183, pp 1404-1417.

5) Waters S., and Aggidis G.S. (2015): *Over 2000 years in review: Revival of the Archimedes Screw from Pump to Turbine*, Renewable and Sustainable Energy Reviews, Vol. 51, pp. 497-505.

6) Songin K. (2017*): Experimental Analysis of Archimedes Screw Turbines*, University of Guelph, Ontario, Canada.